Ultrafast and Sensitive Colorimetric Detection of Ascorbic Acid with Pd-Pt Core-Shell Nanostructure as Peroxidase Mimic

Edwin Davidson,[b] Zheng Xi,[a] Zhuangqiang Gao[a] and Xiaohu Xia*[a,b]

[a] *Department of Chemistry and* [b]*NanoScience Technology Center*, *University of Central Florida, Orlando, Florida 32816, United States*

*Corresponding author. E-mails: Xiaohu.Xia@ucf.edu

Abstract

In recent years, nanostructures with peroxidase-like properties (*i.e.* peroxidase mimics) have attracted special interest due to their low costs, decent stabilities, and high catalytic activities. Herein, we demonstrate the use of Pd-Pt core-shell nanocubes (NCs) as efficient peroxidase mimics to achieve rapid and sensitive colorimetric detection of ascorbic acid (AA, which is commonly known as vitamin C). The color signal generated by the Pd-Pt NCs catalyzed oxidation of 3,3',5,5'-tetramethylbenzidine (TMB) by H_2O_2 is quenched in presence of AA based on its antioxidant property. This colorimetric method attains a detection limit of 0.40 μM and a linear range of 0 to 15 μM, with good linearity. To the best of our knowledge, the method reported in this work presents the fastest AA detection among all the other reported colorimetric methods, with only a 3-minute reaction time. Furthermore, this method features a simple procedure, cost-effectiveness, room temperature conditions and good stability.

Table of Contents

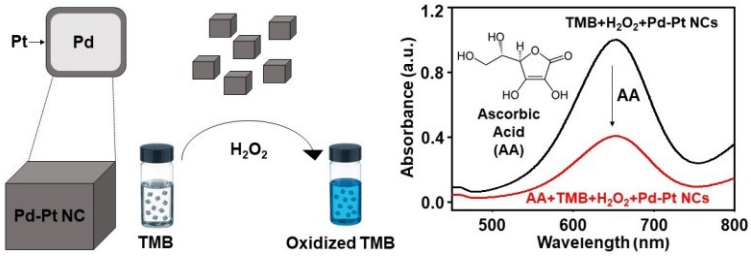

***Keywords*:** nanostructure, peroxidase mimic, colorimetric sensing, ascorbic acid, catalysis.

1. Introduction

Ascorbic acid (AA), also known as vitamin C, is a kind of natural water-soluble vitamin and considered to be an important antioxidant agent and cofactor in enzymatic reactions [1]. It is beneficial in metabolic detoxifying reactions involving reactive oxygen species [2], development of the immune system [3], and the formation of collagen in different tissues of the body [4]. Unfortunately, this relevant vitamin can't be produced by human body, so it must be obtained through daily diet and health supplements. The deficiency of vitamin C will cause scurvy and prompt people to suffer other diseases such as cardio-vascular related diseases [5] or even cancers [6]. Thus, the vitamin C industry has a global market based on the preventive approach of the population to avoid getting the cold or other diseases. Under these circumstances, development of a fast and simple method for detection of vitamin C is highly desirable.

The antioxidant property of AA comes from its reducing power that inhibits oxidation by terminating the chain reactions involved in the oxidation processes [2]. Taking advantage of the reducing power of AA, there have been reported studies using colorimetric assays to determine its concentration [7,8]. The presence of AA inhibits the catalyzed oxidation reaction of a certain substrate, like the 3,3',5,5'-tetramethylbenzidine (TMB), in the presence of hydrogen peroxide (H_2O_2) due to its interaction with the ·OH radicals, resulting in a quench in the formation of colored reaction products [9]. This colorimetric reaction can be prompted with a natural peroxidase (e.g. horseradish peroxidase [10]) or a peroxidase mimic both having the ability to catalyze the oxidation of TMB with H_2O_2.

In recent years, peroxidase mimics have attracted great interest due to their ability to achieve higher catalytic activity than natural enzymes. In addition, they also possess intrinsic advantages such as low cost, mass production, tunable activity, good stability in harsh conditions and long-term storage [11]. Notable examples about the peroxidase mimics developed recently include noble metal nanostructures [12], metal oxides [13], metal-organic frameworks [14,15], carbon-based nanomaterials [16] and so on. Especially, nanostructures of Pt were reported having high catalytic efficiency in the decomposition of dilute aqueous solutions of H_2O_2 among the other kinds of peroxidase mimics [17].

In this work, we demonstrate the development of an enzyme-free colorimetric method for rapid detection of AA with high sensitivity. We chose Pd-Pt core-shell nanocubes (NCs) as active peroxidase mimics because Pt based nanostructures were found to be among the most active

peroxidase mimics and the core-shell structure with thin Pt layer on the surface can maximize its utilization according to our previously published works [18,19]. Herein, the reported Pd-Pt NCs based colorimetric method achieves a low limit of detection of 0.40 μM in only 3 minutes of reaction time. Significantly, less time is needed than other previously reported colorimetric methods which require a longer time to achieve a comparable limit of detection. Furthermore, this approach was performed at room temperature in the aqueous solution, with a simple and fast procedure. The only instrument needed is an inexpensive spectrophotometer because even the naked eye can perceive the colorimetric changes in different concentrations of AA. To the best of our knowledge, this work presents the fastest colorimetric method for AA detection. This method offers the potential application in bio-detection, proving a near-future rapid and sensitive assay for the determination of vitamin C deficiency related diagnosis.

2. Experimental Section

2.1 Chemicals. L-ascorbic acid (AA, 99%), citric acid (99%), sodium tetrachloropalladate (II) (Na_2PdCl_4, 98%), potassium bromide (KBr, 99%), potassium tetrachloroplatinate (II) (K_2PtCl_4, 98%), polyvinylpyrrolidone (PVP, MW ≈ 55,000), 3,3',5,5'-tetramethylbenzidine (TMB, 99%), hydrogen peroxide solution (30% in water), acetic acid (HOAc, 99.7%), sodium acetate (NaOAc, 99%), dopamine hydrochloride (DA), and L-cysteine (Cys, 97%) were all purchased from Sigma-Aldrich. To prepare the aqueous solutions, we used deionized (DI) water with a resistivity of 18.2 MΩ·cm.

2.2 Characterizations and instrumentation. JEOL 1011 microscope operated at 200 kV was used to take the transmission electron microscopy (TEM) images. Agilent Cary 60 UV-vis spectrophotometer was used to measure the UV-vis spectra. PANalytical Empyrean diffractometer (1.8 KW Copper X-ray Tube) was used to record the X-ray Diffraction (XRD) patterns. An Oakton pH 700 benchtop meter was used to measure the pH value of the buffer solution. The Inductively coupled plasma atomic emission spectroscopy (ICP-AES, JY2000 Ultrace ICP atomic emission spectrometer equipped with a JYAS 421 autosampler and 2400 g/mm holographic grating) was used to determine the concentrations of Pd and Pt ions. Using the size and shape from the TEM images, the ionic concentrations were converted to the particle concentration of Pd-Pt NCs. A Canon EOS Rebel T5 digital camera was used to take pictures of the samples in cuvettes.

2.3 Synthesis of Pd nanocubes (NCs) as seeds. These Pd NCs were synthesized according to

our previously reported procedure with minor modifications [18]. For the 7.0 and 18.1 nm Pd NCs, the procedure consisted of 60 mg of AA, 105 mg of PVP, different amounts of KBr and KCl depending on the desired size (8 mg of KBr and 180 mg of KCl for 9.0 nm Pd NCs; 600 mg of KBr and 180 mg of KCl for 18.1 nm Pd NCs) all together in a vial and then it was pre-heated to 80 °C for 10 minutes in an oil bath under magnetic stirring. Next, 3 mL of Na_2PdCl_4 aqueous solution with a concentration of 19 mg/mL was rapidly added. Lastly, the mixture was allowed to react for 3 hours and then it was cooled down to room temperature to be washed three times and the final product was redispersed in 8 mL of deionized (DI) water for future use.

For the 40.3 nm Pd NCs, Pd NCs of 18.1 nm were used as seeds to mediate the growth into larger NCs. The procedure consisted of 90 mg of AA, 150 mg of PVP, 450 mg KBr and 0.72 mL of the previously synthesized Pd seeds all together in a flask and then it was pre-heated to 40 °C for 20 minutes in an oil bath under magnetic stirring. Subsequently, 5 mL of Na_2PdCl_4 aqueous solution with a concentration of 19 mg/mL was rapidly added. Next, the mixture was allowed to react for 24 hours and then it was cooled down to room temperature to be washed three times and the final product was redispersed in 5 mL of deionized (DI) water for future use.

2.4 Synthesis of Pd-Pt NCs. After the synthesis of the Pd NCs, they were used as seeds to deposit a thin layer of Pt atoms as shell, following the previously reported method with minor modifications [20]. The standard synthesis procedure consisted of 60 mg of citric acid, 35 mg of PVP and 5 mL of previously synthesized 40.3 nm Pd NC solution, dissolved in a total volume of 10 mL DI water in a glass vial and then preheated to 95 °C for 10 minutes under magnetic stirring. Subsequently, 3 mL of K_2PtCl_4 solution with a concentration of 4.33 mg/mL was rapidly added. Next, the mixture was allowed to react for 24 hours and then it was cooled down to room temperature to be washed three times and the final product was redispersed in 5 mL DI water. The same procedure was followed to synthesize the 9.0 and 20.3 nm of Pd-Pt except for the use of different sizes of Pd seeds (7.0 and 18.1 nm) with a 3 mL K_2PtCl_4 solution with concentrations of 0.75 and 1.95 mg/mL, respectively.

2.5 Steady-State kinetics assay. We followed our previously published procedures [18,21]. The procedure consisted of a standard catalytic reaction initiated by mixing Pd-Pt NC catalysts with varying concentrations of TMB and H_2O_2 in a solution buffer 0.2 M NaOAc/HOAc (pH = 4.0) in a 1.0 mL cuvette (with a path length of 1.0 cm) at room temperature conditions. Then, the cuvette was placed in the UV-vis spectrophotometer to gather the absorbances at 653 nm as a function of

time in 2-second interval for 1 minute. This procedure was used to evaluate two substrates consisting one assay for H_2O_2 by fixing the concentration of TMB and varying the H_2O_2 concentration, and the other assay for TMB by doing the opposite, fixing the H_2O_2 concentration and varying the TMB concentration to obtain the "absorbance *vs* time" plots. Then we calculated the initial points ($Slope_{initial}$) of each curve by conducting the first derivation. Next, the initial reaction velocity (v) was calculated with the formula: $Slope_{initial}/(\varepsilon_{TMB\text{-}653nm} \times l)$, where l is the path length and $\varepsilon_{TMB\text{-}653nm}$ is the molar extinction coefficient of oxidized TMB at 653 nm (which is 3.9×10^4 $M^{-1}\cdot cm^{-1}$). All of the initial reaction velocity (v) against substrate concentrations ([S]) plots were then fitted using nonlinear regression of the Michaelis-Menten equation, $v = V_{max} \times [S]/(K_m + [S])$. Lastly, we determined the kinetic parameters K_m and V_{max} (where V_{max} is the maximal reaction velocity, and K_m is the Michaelis constant) obtained from the Lineweaver–Burk double reciprocal plot generated from the Michaelis−Menten equation. After determining the V_{max}, the catalytic constant (K_{cat}) was derived from the equation $K_{cat} = V_{max}/[E]$, where $[E]$ represents the Pd-Pt NCs concentration.

2.6 Colorimetric detection of AA with Pd-Pt NCs. The procedure consisted in the use of AA standards with various concentrations in a range from 0 to 15 μM. Then, to a disposal plastic cuvette, 275 μL H_2O_2 (in 2 M concentration), 200 μL HOAc/NaOAc buffer (pH = 4.0), 10 μL of Pd-Pt NCs (in a concentration of 4.2×10^9 particles/ mL, ~7.0×10^{-12} M) and 500 μL of AA standard solution were added. Subsequently, 15.4 μL TMB (in 52 mM concentration) is added and mixed all together for 3-minute incubation at room temperature, then proceeded to measure the absorbance spectra with a UV-vis spectrophotometer and take photographs with a digital camera.

2.7 Selectivity for ascorbic acid detection. To evaluate the selectivity of our Pd-Pt NCs toward AA detection, we followed our proposed method, with the addition of 500 μL interferential substances. The interferential substances were prepared by dissolving Na_2CO_3, $CaSO_4$, K_3PO_4, dopamine hydrochloride, L-cysteine and D-glucose in DI water to obtain the 1 mM solution of Na^+, Ca^{2+}, K^+, glucose and the 100 μM solution of dopamine and cysteine, respectively. All the chemicals were analytical grade and were used as received without further purification.

3. Results and Discussion

3.1 Structure and composition study. We started with the synthesis of Pd-Pt core-shell NCs. The synthesis was achieved through a two-step seed-mediated growth. First, the monodispersed

40.3 nm Pd NCs (Figure 1A) were initially synthesized and utilized as seeds according to the method published by our group [18]. Second, in a standard synthesis of Pd-Pt core-shell NCs, the aqueous solution of K_2PtCl_4 as the Pt precursor was quickly injected into the mixture containing 40.3 nm Pd NCs as seeds, citric acid as reducing agent and poly(vinylpyrrolidone) ($M_w \approx 55{,}000$) as surfactant, which was mixed under magnetic stirring and preheated to 95 °C in a vial through the oil bath. The reaction was allowed to proceed for 24 h (see details in Experimental Section). After the successful deposition of Pt layers on the surface of the Pd NCs, they kept the overall cubic shape and increased the average edge length to 42.3 nm, as shown in the transmission electron microscopy (TEM) images in Figure 1B and 1C. The molar ratio of Pt to Pd was determined to be ~0.155 using inductively coupled plasma atomic emission spectroscopy (ICP-AES). This data along with the size/shape of nanoparticles indicated the thickness of the Pt layer was approximately 1 nm. The ~1 nm Pt shell can also be seen in the high-resolution TEM (HRTEM) image in Figure 1D, where Pt displayed a darker contrast than Pd [20]. Notably, the periodic lattice fringes in Figure 1D was measured to be 1.91 Å, corresponding to the (200) planes of Pd NCs, indicating the exposure of six {100} facets for the cubic shape. The successful formation of the Pd-Pt NCs was further confirmed with an X-ray diffraction (XRD) pattern as shown in Figure 1E. All the diffraction peaks could be assigned to the face-centered cubic (*fcc*) Pd (JCPDS no. 46-1043) without obvious Pt diffraction peaks, indicating the successful formation of thin Pt layer on Pd surface without the self-nucleation of extra Pt nanoparticles [22].

Moreover, the size of the Pd-Pt core-shell NCs can be controlled by using Pd NCs of different sizes as seeds. For demonstration, Pd NCs of two different sizes were successfully synthesized (Figures S1A and S1B, 7.0 nm and 18.1 nm, respectively), which can be used as seeds to obtain the Pd-Pt core-shell NCs (Figure S1C and S1D) with average sizes of 9.0 nm and 20.3 nm, respectively. From the enlargement of the NC sizes before and after Pt coating, the Pt shell thicknesses for the two Pd-Pt NCs were both approximately 1 nm, similar to the 42.3 nm Pd-Pt NCs.

3.2 Peroxidase-like activities. To evaluate the peroxidase-like properties for the synthesized Pd-Pt NCs, the steady-state kinetic assays were performed as a simple and rapid method for assessing the catalytic efficiency. The oxidation of TMB by H_2O_2 was used as a model reaction because it yields a blue-colored product from the oxidized TMB with a characteristic peak at λ_{max} = 653 nm [10]. The kinetic assay procedure published by our group consisted in a standard catalytic

reaction initiated by mixing certain amount of Pd-Pt NCs as catalysts (see Table 1) with varying concentrations of TMB and H_2O_2 in the solution buffer 0.2 M NaOAc/HOAc (pH = 4.0) in a 1.0 mL cuvette (with path length of 1.0 cm) at room temperature [18,21]. Then, the cuvette was immediately measured by the UV-vis spectrophotometer to gather the initial reaction velocities (see details in Experimental Section). Afterward, the initial reaction velocities against substrate concentrations were plotted to obtain the typical Michaelis-Menten curves obtained in Figure 2 and S2 for TMB and H_2O_2 as substrate, respectively. Then, as shown in the insets of each figure, the curves were fitted using the Lineweaver–Burk double reciprocal from the Michaelis-Menten plots to calculate the kinetics parameters summarized in Table 1. As summarized in Figure 3, the K_{cat} value (defined as the maximum number of substrate conversions per second per catalyst) increases with the enlargement of the Pd-Pt NC sizes, with the 42.3 nm being the largest one (K_{cat} = 9.4×10^6 s^{-1} for TMB and 7.6×10^6 s^{-1} for H_2O_2, respectively). This increase in catalytic activity may be attributed to the increase of surface area in larger NCs covered with a greater area of Pt which have higher catalytic activity in peroxidase reactions [17]. Notably, the 42.3 nm Pd-Pt NCs were about 1,000-folds higher than horseradish peroxidase (HRP) [13].

3.3 Colorimetric detection of ascorbic acid. The detection of AA is based on its antioxidant property of inhibiting oxidation processes by quenching the reactive free radicals [9]. The TMB when oxidized yields a blue-colored complex with an absorbance peak at 653 nm. However, in the presence of AA, this peak presents a proportional decrease in absorbance as a function of the concentration of AA caused by the retarded formation of the blue solution. The aforementioned detection principle is shown in Figure 4A with the proportional decrease of absorbance at different AA concentrations.

Before evaluating the sensitivity of our method, the conditions to conduct the detection were established based on the previous work from our group with optimal conditions for the TMB oxidation with H_2O_2, (*i.e.* 0.2 M pH 4.0 NaOAc/HOAc buffer solution, 0.8 mM TMB and 2 M H_2O_2 at room temperature) [12,18,19]. In regard, to determine the reaction time of this detection method, we evaluated the difference of absorbances (ΔA) against incubation time in a range from 1 to 15 minutes, in which we found 3 minutes to be optimal reaction time with a higher difference between the absorbance without the analyte (A_0) and the absorbance in the presence of the analyte (A_x), as shown in Figure S3A. The variables A_0 and A_x refer to the absorbances at 653 nm of the blank solution and the AA standard solution of x μM, respectively. Furthermore, we generated

three calibration curves by plotting A_0-A_x as a function of the AA concentrations, each curve corresponds to different reaction time (3, 5 and 7 minutes) to evaluate the reaction time with higher sensitivity and detection range (see Figure S3B). Unsurprisingly, the 7 minutes reaction curve achieved a greater detection range allowing higher concentrations of AA to be detected because waiting for longer time allows solutions with higher concentrations of AA to eventually develop the blue-colored signal. However, the lowest limit of detection was achieved with the 3-minute reaction curve. The 3-minute calibration curve for AA detection shows a good correlation between the decrease in absorbance A_0-A_x against AA concentration. Therefore, reaction time of 3 minutes was chosen as a standard condition for the detection. In addition to reaction time, we also evaluated the impact of concentration of Pd-Pt NCs. As shown in Figure S4, the optimal concentration of Pd-Pt NCs was found to be 7.0×10^{-14} M. A higher or lower concentration of Pd-Pt NCs led to increased LOD for AA detection. As shown by Figures 4B and 4C, respectively, this method has a detection range from 0 to 50 μM and a linear range from 1 to 15 μM with good linear relationship of $R^2 = 0.996$. The limit of detection (LOD, defined as the concentration corresponding to a signal that is 3 times the standard deviation above the zero-calibration point [23]) was calculated to be 0.40 μM with a good reproducibility (n = 6). Compared with other AA colorimetric detection methods using nanoparticles, this work not only showed a very low detection limit but also had the shortest reaction time (see Table 2 for the comparison). It is worth mentioning that materials cost of noble metals should not be an issue in this particular application because of the tiny usage amount of noble-metal nanoparticles per test (approximately nanogram level of Pd and Pt).

3.4 Selectivity for ascorbic acid detection. To evaluate the selectivity of our method to AA detection, we investigated the interference of dopamine (DA) because it is an analog of AA that naturally co-exists together in human blood and [7]. We also examined potential interference of thiol by testing cysteine (Cys) as a common type of amino acid that contains thiol group [24]. Figures 5A shows the slight decrease in the 653 nm peak intensity with the addition of 100 μM DA and Cys. However, with the addition of 100 μM AA, there is a significant decrease in the absorbance of the peak, which corroborates the good selectivity of the Pd-Pt NCs based method towards the detection of AA.

Furthermore, we also investigated the interference of 1 mM concentration of common ions (Na^+, K^+, and Ca^{2+}) and 1 mM concentration of glucose, a commonly present small biological molecule in blood, by measuring the absorbance response of the detection system in the presence

of the interference. As observed in the results of Figure 5B, there was no remarkable influence in the absorbance of the 653 nm peak intensity of the control upon the addition of interferential substances. In comparison, the presence of 1 mM AA induced a significant reduction of absorbance at 653 nm. These results demonstrated the excellent specificity of our method towards the colorimetric detection of ascorbic acid, reassuring its sensing applicability to biological samples testing.

Conclusion

In summary, this work has demonstrated an ultrafast and sensitive colorimetric detection of ascorbic acid that was developed based on the peroxidase-like activity of Pd-Pt NCs. Such Pd-Pt NCs based colorimetric method also features a simple detection procedure, low cost, fast operation, and high stability. This method has been successfully applied to the detection of ascorbic acid in aqueous solutions. We believe the method presented in this work may find widespread use in detection of ascorbic acid (Vitamin C) in various samples.

Acknowledgments

This work was supported in part by grants from the National Science Foundation (CHE-1834874), and the startup funds from University of Central Florida (UCF). Z.X. was partially supported by the UCF Preeminent Postdoctoral Program. E.D. was supported by the Fulbright Scholarship Program.

Conflict of Interest

The authors declare no conflict of interest.

References

1. W. J. Liang, D. Johnson, S. M. Jarvis, Vitamin C transport systems of mammalian cells, Mol. Membr. Biol. 18 (1) (2001) 87-95.
2. O. Arrigoni, M. C. De Tullio, Ascorbic acid: much more than just an antioxidant, Biochim. Biophys. Acta. 1569 (1-3) (2002) 1-9.

3. A. Ströhle, A. Hahn, Vitamin C and immune function, Med. Monatsschr. Pharma. 32 (2) (2009) 49-54.
4. W. B. Robertson, B. Schwartz, Ascorbic acid and the formation of collagen, J. Biol. Chem. 201 (1953) 689-696.
5. J. Simon, Vitamin C and cardiovascular disease: a review, J. Am. Coll. Nutr. 11 (2) (1992) 107-125.
6. G. Block, Vitamin C and cancer prevention: the epidemiologic evidence, Am. J. Clin. Nutr. 53 (1) (1991) 270S-282S.
7. G. Darabdhara, B. Sharma, M. R. Das, R. Boukherroub, S. Szunerits, Cu-Ag bimetallic nanoparticles on reduced graphene oxide nanosheets as peroxidase mimic for glucose and ascorbic acid detection, Sensor Actuat. B Chem. 238 (2017) 842-851.
8. H. Tan, C. Ma, L. Gao, Q. Li, Y. Song, F. Xu, T. Wang, L. Wang, Metal–organic framework-derived copper nanoparticle@carbon nanocomposites as peroxidase mimics for colorimetric sensing of ascorbic acid, Chem. Eur. J. 20 (49) (2014) 16377-16383.
9. X. Wang, Q. Han, S. Cai, T. Wang, C. Qi, R. Yang, C. Wang, Excellent peroxidase mimicking property of CuO/Pt nanocomposites and their application as an ascorbic acid sensor, Analyst. 142 (13) (2017) 2500-2506.
10. P. D. Josephy, T. Eling, R. P. Mason, The horseradish peroxidase-catalyzed oxidation of 3,5,3',5'-tetramethylbenzidine. Free radical and charge-transfer complex intermediates, J. Biol. Chem. 257 (1982) 3669-3675.
11. H. Wei, E. Wang, Nanomaterials with enzyme-like characteristics (nanozymes): next-generation artificial enzymes, Chem. Soc. Rev. 42 (14) (2013) 6060-6093.
12. Z. Gao, G. G. Liu, H. Ye, R. Rauschendorfer, D. Tang, X. Xia, Facile colorimetric detection of silver ions with picomolar sensitivity, Anal. Chem. 89 (6) (2017) 3622-3629.
13. L. Gao, J. Zhuang, L. Nie, J. Zhang, Y. Zhang, N. Gu, T. Wang, J. Feng, D. Yang, S. Perrett, X. Yan, Intrinsic peroxidase-like activity of ferromagnetic nanoparticles, Nat. Nanotech. 2 (9) (2007) 577–583.
14. J. W. Zhang, H. T. Zhang, Z. Y. Du, X. Wang, S. H. Yu, H. L. Jiang, Water-stable metal-organic frameworks with intrinsic peroxidase-like catalytic activity as a colorimetric biosensing platform, Chem. Commun. 50 (9) (2014) 1092-1094.

15. L. Ai, L. Li, C. Zhang, J. Fu, J. Jiang, MIL-53 (Fe): a metal–organic framework with intrinsic peroxidase-like catalytic activity for colorimetric biosensing, Chem. A Eur. J. 19 (45) (2013) 15105-15108.
16. Y. Jiang, N. Song, C. Wang, N. Pinna, X. Lu, A facile synthesis of Fe_3O_4/nitrogen-doped carbon hybrid nanofibers as a robust peroxidase-like catalyst for the sensitive colorimetric detection of ascorbic acid, J. Mater. Chem. B. 5 (27) (2017) 5499-5505.
17. D. W. McKee, Catalytic decomposition of hydrogen peroxide by metals and alloys of the platinum group, J. Catal. 14 (4) (1969) 355-364.
18. X. Xia, J. Zhang, N. Lu, M. Kim, K. Ghale, Y. Xu, E. McKenzie, J. Liu, H. Ye, Pd–Ir core–shell nanocubes: a type of highly efficient and versatile peroxidase mimic, ACS Nano. 9 (10) (2015) 9994-10004.
19. H. Ye, Y. Liu, A. Chhabra, E. Lilla, X. Xia, Polyvinylpyrrolidone (PVP)-capped Pt nanocubes with superior peroxidase-like activity, ChemNanoMat. 3 (1) (2017) 33-38.
20. J. Park, L. Zhang, S. I. Choi, L. T. Roling, N. Lu, J. A. Herron, S. Xie, J. Wang, M. J. Kim, M. Mavrikakis, Y. Xia, Atomic layer-by-layer deposition of platinum on palladium octahedra for enhanced catalysts toward the oxygen reduction reaction, Nano Lett. 14 (6) (2014) 3570-3576.
21. Z. Xi, X. Cheng, Z. Gao, M. Wang, T. Cai, M. Muzzio, E. Davidson, O. Chen, Y. Jung, S. Sun, Y. Xu, X. Xia, Strain effect in palladium nanostructures as nanozymes, Nano Lett. 20 (1) (2020) 272–277.
22. BT Sneed, AP Young, D Jalalpoor, MC Golden, S Mao, Ying Jiang, Yong Wang, and Chia-Kuang Tsung, Shaped Pd–Ni–Pt Core-Sandwich-Shell Nanoparticles: Influence of Ni Sandwich Layers on Catalytic Electrooxidations, ACS Nano. 8 (7) (2014) 7239-7250.
23. D. A. Armbruster, M. D. Tillman, L. M. Hubbs, Limit of detection (LQD)/limit of quantitation (LOQ): comparison of the empirical and the statistical methods exemplified with GC-MS assays of abused drugs, Clin. Chem. 40 (7) (1994) 1233-1238.
24. Y. S. Borghei, M. Hosseini, M. Khoobi, M. R. Ganjali, Novel fluorometric assay for detection of cysteine as a reducing agent and template in formation of copper nanoclusters, J. Fluoresc. 27 (2) (2017) 529-536.
25. L. P. Zhang, B Hu, JH Wang, Label-free colorimetric sensing of ascorbic acid based on Fenton reaction with unmodified gold nanoparticle probes and multiple molecular logic gates, Anal. Chim. Acta. 717 (2012) 127-133.

26. Y. Jiang, N. Song, C. Wang, N. Pinna, X. Lu, Sensitive colorimetric detection of ascorbic acid using Pt/CeO_2 nanocomposites as peroxidase mimics, Appl. Surf. Sci. 479 (2019) 532-539.
27. L. He, F. Wang, Y. Chen, Y. Liu, Rapid and sensitive colorimetric detection of ascorbic acid in food based on the intrinsic oxidase-like activity of MnO_2 nanosheets, Luminescence. 33 (1) (2018) 145-152.
28. L. Lin, Y. Luo, Q. Chen, Q. Lai, Q. Zheng, Redox-modulated colorimetric detection of ascorbic acid and alkaline phosphatase activity with gold nanoparticles, Luminescence. 35 (4) (2020) 542-549.

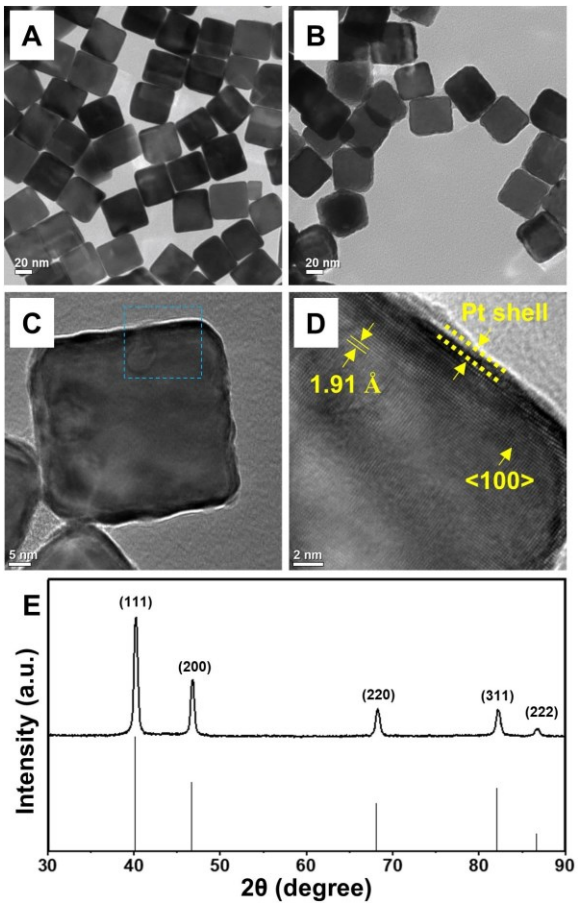

Figure 1. Structural analyses of the Pd-Pt NCs. (A) TEM image of 40.3 nm Pd NCs. (B) and (C) TEM images of 42.3 nm Pd-Pt NCs. (D) HRTEM image of Pd-Pt core-shell NC taken from the region near the blue box in (C). (E) Powder XRD spectra recorded from the Pd-Pt NCs (black bars represent standard Pd XRD diffraction pattern, JCPDS no. 46-1043).

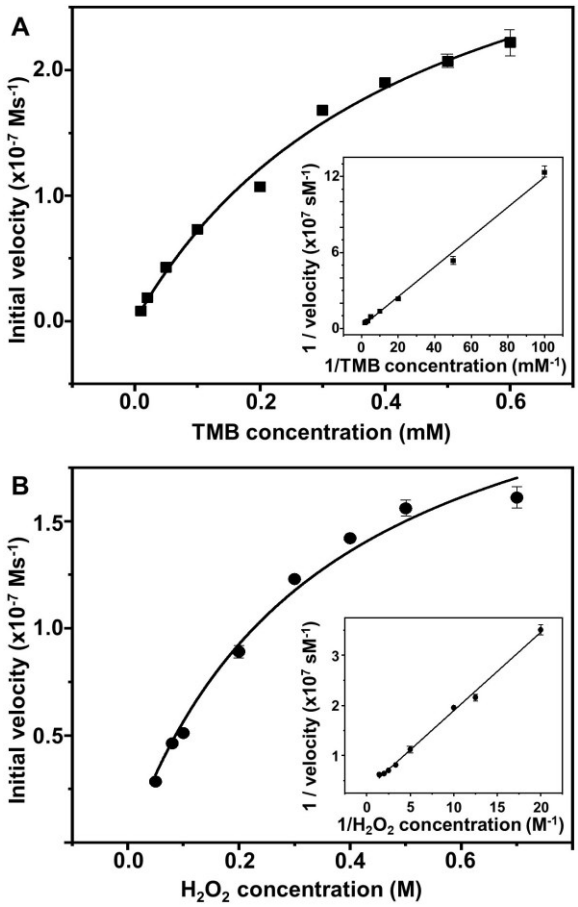

Figure 2. Steady-state kinetic assays of the 42.3 nm Pd-Pt NCs as catalysts for the oxidation of TMB by H_2O_2. (A) Plot of initial velocity against TMB concentration, where the concentration of H_2O_2 was fix to 2 M. (B) Plot of initial velocity against H_2O_2 concentration, where the concentration of TMB was fix to 0.8 mM. Insets: Double-reciprocal plots generated from corresponding curves. Error bars indicate the standard deviation from three independent measurement.

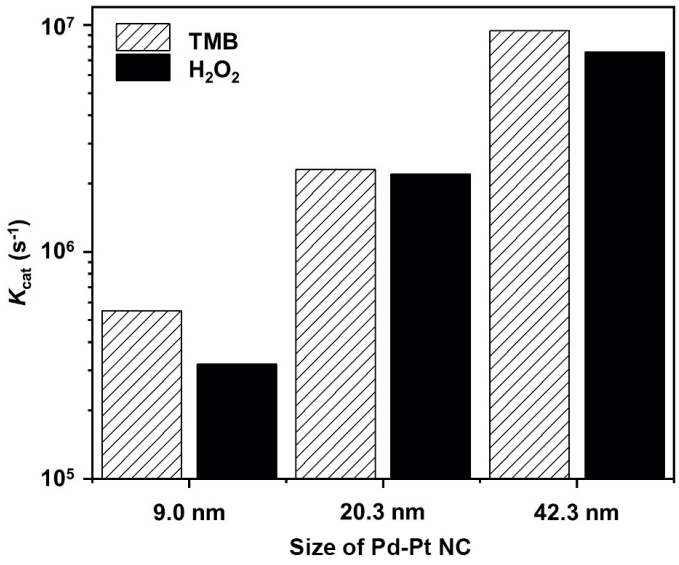

Figure 3. Size effect in the Pd-Pt NCs catalyzed oxidation of TMB by H_2O_2. The histogram compares the K_{cat} values of different sized Pd-Pt NCs toward TMB and H_2O_2.

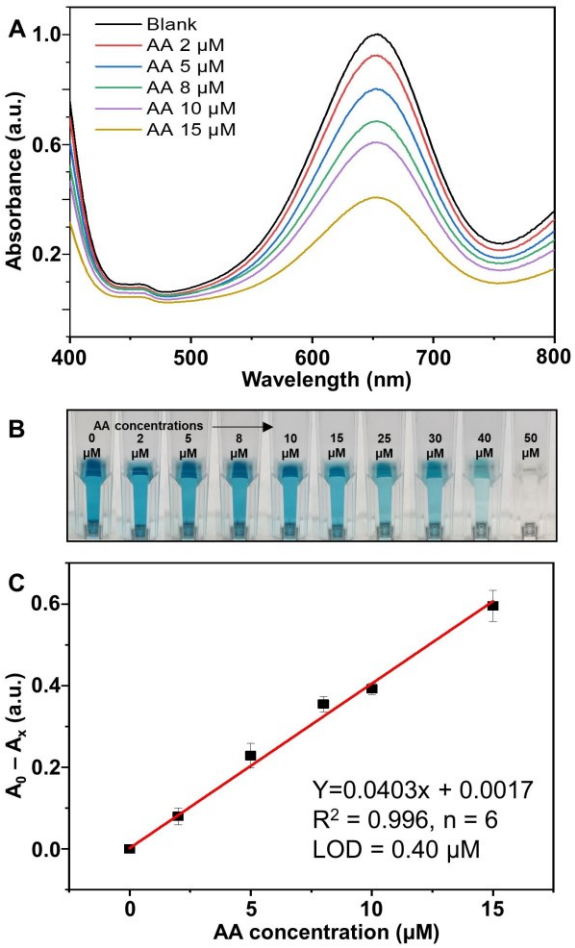

Figure 4. Detection of AA standards using the Pd-Pt NCs based colorimetric method. (A) Effects of AA concentrations on the UV-Vis absorption spectra of the Pd-Pt NCs catalyzed reaction solution containing TMB and H_2O_2. (B) Color changes of the Pd-Pt NCs catalyzed reaction solutions in the presence of AA with different concentrations after 3-minute reaction. (C) Calibration curve generated by plotting the decrease of the absorbance at 653 nm A_0-A_x as a function of AA concentration, where A_0 and A_x refer to the absorbances of the blank solution and the solution containing x μM of AA, respectively. Error bars indicate the standard deviations of six independent measurements.

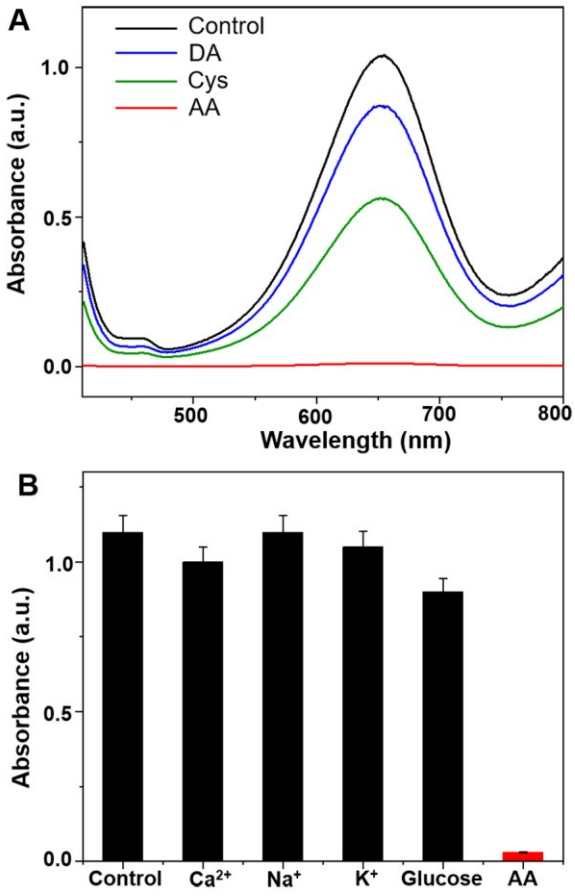

Figure 5. Selectivity for the Pd-Pt NCs based colorimetric detection of AA. (A) UV-vis spectra of the detection system in the presence of 100 μM dopamine (DA), cysteine (Cys) and ascorbic acid (AA). (B) Intensities of the absorbances at 653 nm that were determined from the detection system in the presence of various interferential substances. The interferential substance concentrations are all 1 mM. The error bars indicate the standard deviations of three independent measurements.

Table 1. Comparison of the kinetic parameters of Pd-Pt NCs with different sizes towards the oxidation of TMB by H_2O_2.

Substrate	Size of Pd-Pt NC (nm)	$[E]^{[a]}$ (M)	$K_m^{[b]}$ (M)	$V_{max}^{[c]}$ (M/s)	$K_{cat}^{[d]}$ (s^{-1})
TMB	9.0	1.3×10^{-12}	4.8×10^{-4}	7.1×10^{-7}	5.5×10^{5}
H_2O_2		1.3×10^{-12}	3.9×10^{-1}	4.2×10^{-7}	3.2×10^{5}
TMB	20.3	2.6×10^{-13}	3.4×10^{-4}	6.0×10^{-7}	2.3×10^{6}
H_2O_2		2.6×10^{-13}	7.7×10^{-1}	5.8×10^{-7}	2.2×10^{6}
TMB	42.3	3.4×10^{-14}	4.5×10^{-4}	3.2×10^{-7}	9.4×10^{6}
H_2O_2		3.4×10^{-14}	3.5×10^{-1}	2.6×10^{-7}	7.6×10^{6}

[a] represents Pd-Pt NC particle concentration, [b] represents the Michaelis-Menten constant, [c] represents the maximal reaction velocity, and [d] represents catalytic constant that measures the catalytic activity.

Table 2. Comparison of analytical performances of various colorimetric methods for ascorbic acid (AA) detection.

Catalyst	LOD[a] (μM)	Reaction Time (min)	Ref.
Cu-Ag/rGO	3.6	50	[7]
Cu nanoparticles-Carbon	1.4	20	[8]
MIL-68/MIL-100	6	~10	[14]
MIL-53 (Fe)	15	15	[15]
Fe_3O_4/nitrogen-doped carbon (Fe_3O_4/N-C) hybrid nanofibers	0.04	10	[16]
Au nanoparticles-DNA	0.3	30	[25]
Pt/CeO_2 nanocomposites	0.08	10	[26]
Single-layered MnO_2 nanosheets	0.063	5	[27]
ALP-Au nanoparticles	2.44	75	[28]
Pd-Pt nanocubes	0.40	3	This work.

[a] denotes the limit of detection.